

Thermal Hall Conductance of an Isolated Non-Abelian Edge Mode

Bivas Dutta, Vladimir Umansky, and Moty Heiblum*

Braun Center for Sub-Micron Research, Department of Condensed Matter Physics,

Weizmann Institute of Science, Rehovot, Israel 76100

*e-mail: moty.heiblum@weizmann.ac.il

Non-abelian anyons are prospective candidates for fault-tolerant topological quantum computation. Curiously these non-abelian modes are charge neutral, which makes them elusive to most of the conventional measurement techniques. Among others, a proposed host of such quasiparticles is the $\nu=5/2$ quantum Hall effect (QHE) state. Recent measurements of the state's thermal conductance G_{th} found a half-integer of the expected universal value for an abelian state¹. However, the ambiguity about inter-mode thermal equilibration among all edge modes of $\nu=5/2$ remains open. Since most of predicted non-abelian QHE states co-host both abelian and non-abelian edge modes, a robust technique is needed to isolate the non-abelian modes and subsequently test their non-abelian character, in order to have their access into non-abelian braiding (interference), a primary step for non-abelian topological quantum processing. In this paper, we address this particular issue. We exploit a novel technique² to gap-out the integer modes by interfacing the $\nu=5/2$ state with a nearby integer state ($\nu=2$ & $\nu=3$); allowing a direct measurement of the fully equilibrated, isolated $\nu=1/2$ charge mode accompanied with a Majorana mode. Observing $G_{\text{th}} = 0.5\kappa_0 T$ (with $\kappa_0 = \pi^2 k_B^2 / 3h$), assures the non-abelian nature of the $\nu=5/2$ state and its particle-hole Pfaffian topological order. Our result opens new avenue to manipulate and test other QHE states, as well as to braid, via interference, the isolated exotic modes.

Fractional quantum Hall effect states support localized fractionally charged quasiparticles in the bulk and gapless conducting edge modes. The Laughlin states and their particle-hole conjugated states are abelian, while their exotic cousins, having a highly degenerate ground state with an exponential degeneracy in the number of quasiparticle excitations, are non-abelian^{3,4}. The latter may permit different topological orders that support non-Bosonic upstream neutral modes, invisible to ubiquitous conductance measurements⁵. The thermal Hall conductance $G_{\text{th}} = KT$, with T the temperature, is sensitive to all energy-carrying modes, and thus, a vital system characteristic and a topological invariant that depends only on the bulk of the system. Measured at the edge (with the 'bulk-edge correspondence'), the thermal Hall conductance strongly depends on the thermal-equilibration between the counter-propagating edge modes. In the abelian regime, with downstream (DS) and upstream (US) modes fully equilibrated, the thermal

conductance is given by $KT = (n_d - n_u)\kappa_0 T$, with $\kappa_0 = \pi^2 k_B^2 / 3h$ the quantum of thermal conductance, k_B the Boltzmann's constant, h the Planck's constant, and n_d (n_u) is the number of downstream (upstream) edge modes. However, in the absence of thermal equilibration, one expects $KT = (n_d + n_u)\kappa_0 T$ ⁶. Note that, similar thermal-equilibration dependence is also expected in the non-abelian regime, but here KT comes with fractional multiples of $\kappa_0 T$, originating from the fractional nature of the chiral central charge⁷.

Recent measurements of the thermal conductance of the $\nu=5/2$ state found $K=2.5\kappa_0$ ¹; suggesting to the 'particle-hole Pfaffian' (PH-Pf) topological order. However, numerical studies^{8,9}, which include Landau-levels mixing (but neglect disorder), favor the non-abelian Pfaffian (Pf) or its particle-hole conjugated, the Anti-Pfaffian (A-Pf) order¹⁰⁻¹². With an upstream neutral mode detected in the $\nu=5/2$ state^{13,14}, the A-Pf, with an expected $K=1.5\kappa_0$, remained the theoretically favored order^{15,16}. Several theoretical models were proposed to resolve the discrepancy between the theory and the experiment. Inhomogeneity of the density may lead to islands of local Pf and A-Pf orders, from which a global PH-Pf order may emerge¹⁷⁻²¹. On the other hand, an unequilibrated neutral Majorana mode in the A-Pf order may lead to the same thermal conductance as that of the PH-Pf order²²⁻²⁵. Therefore, the past thermal conductance experiments, which measured at the sample's physical-edge^{1,26,27}, cannot unambiguously identify the topological order of the $\nu=5/2$ state.

We recently developed a novel method that allows measurements on a gate-defined interface between different quantum Hall effect states², instead of the sample's physical edge. Measuring the thermal conductance of the interface mode between $\nu=5/2$ and $\nu=2$ or $\nu=3$ states, comprising of a $\nu=1/2$ charge mode and neutral Majorana mode(s), we find an equilibrated $KT \cong 0.5\kappa_0 T$, which agrees with the non-abelian PH-Pf topological order.

High quality GaAs-AlGaAs heterostructures with shallow-DX-centers doping, allowing 'hysteresis free' gating and negligible bulk heat conductance at millikelvin temperatures, was grown by MBE². This particular doping leads to stronger disorder compared to conventional superlattice (SPSL) doping^{1,28}. Our experimental setup, with the 'heart' of the fabricated two-arm device is shown in **Fig. 1a**. The inner (yellow) and the outer (violet) gates tune the bulks' filling factors. The gates are isolated from the sample and from each other by 15-25nm thick HfO₂ (for more details, see **Methods**). Gate voltage in the range $-1.5V < V_g < +0.3V$ allowed varying the electron density from pinch-off to $3 \times 10^{11} \text{ cm}^{-2}$ (see **Extended Data Fig. 1**); thus controlling the filling factor. The resulting interface modes split when leaving a small floating ohmic contact ($20 \times 2 \mu\text{m}^2$), which serves as a heated reservoir and connects the two arms (shown in red), and large ohmic contacts (S, D, G, shown in cyan) are placed at the interfaces. Separate contacts at the physical edge of the mesa (not shown) probe the filling factors of each respective region.

Current I_S is injected from S and dissipates power $\Delta P = \frac{1}{4}I_S^2 R_S$ in the floating contact (R_S the two-terminal resistance of the interface). **Figure 1b** provides a schematic representation of the heat balance in the floating contact at the interface. Heat leaving the floating contact is composed of a phononic contribution $\Delta P_{ph} = \beta(T_m^5 - T_0^5)$ and an electronic $\Delta P_e = 0.5K(T_m^2 - T_0^2)$. At equilibrium, $\Delta P = \Delta P_{ph} + \Delta P_e$, with T_m the temperature of the floating contact and T_0 the base temperature. The phononic contribution is negligible at $T_m < 20\text{mK}$. The temperature T_m is determined by measuring the ‘low frequency’ Johnson-Nyquist thermal noise at the drain contact D , which is placed about $160\mu\text{m}$ away along downstream in one arm (see **Methods**). The noise is filtered by an LC resonant circuit (resonance frequency 630 kHz and bandwidth 10-30kHz), amplified by a cold voltage pre-amplifier (placed at 4.2K plate), and a room temperature amplifier.

The general strategy of our experiment is to tune the inner regions to the ‘tested’ state ν_{in} (e.g., $5/2$), and the outer regions to an integer state ν_{out} (e.g., 0, 1, 2, 3); leading to an ‘interface mode filling’ $\nu_{int} = \nu_{in} - \nu_{out}$ (with the nomenclature ‘ $\nu_{in} - \nu_{out}$ ’). The chirality of the interface charge mode reverses when the interfacing condition changes from $\nu_{in} > \nu_{out}$ to $\nu_{in} < \nu_{out}$. With a single downstream amplifier, the magnetic field is reversed between these two cases (see **Methods**).

We start with measurements of interface modes formed in the configurations ‘3-2’, ‘3-1’ and ‘3-0’. The two-probe source resistance exhibits quantized plateaus as a function of the gate voltage, h/e^2 , $h/2e^2$, and $h/3e^2$ ($\sim 0.1\%$ accuracy), respectively. In these chiral configurations, the downstream modes are equilibrated at temperature T_m . The expected thermal conductances are $1\kappa_0 T$, $2\kappa_0 T$, and $3\kappa_0 T$, respectively^{26,27}. The thermal noise measured at the drain S_{th} and the deduced temperature of the floating contact T_m (See **Methods**) are plotted as function of the source current I_S and the dissipated power ΔP respectively in **Figs. 2a & 2b**. We analyze the data in two ways: *i*. By fitting the linear-electronic contribution, ΔP versus T_m^2 for $T_m < 18\text{mK}$, and find $K = 1\kappa_0$, $2\kappa_0$, and $3\kappa_0$, respectively (**Fig. 2c**); *ii*. By fitting the data for $T_m < 30\text{mK}$, which reflects the electronic and phononic contributions. A similar quantization of the thermal conductance is found with $\beta \approx 5 \times 10^9 \text{WK}^{-5}$.

Interfacing $\nu = 7/3$, $5/2$, and $8/3$ with $\nu = 2$ and $\nu = 3$, leads to a two-terminal source resistance (R_S) shown in **Fig. 3a**. Well-quantized plateaus indicate full charge equilibration at the interfaces. We start with the $\nu = 7/3$ and $8/3$ abelian states. Interfacing these two states with $\nu = 2$ results in a $\nu = 1/3$ and a $\nu = 2/3$ modes, respectively (the latter is accompanied by an upstream neutral mode). The interface fillings for the two states are reversed when interfaced with $\nu = 3$ instead: the $\nu = 2/3$ charge accompanied by a neutral mode appears for the $\nu = 7/3$ state, and a single $\nu = 1/3$ charge mode appears for the $\nu = 8/3$ state. The

measured two-terminal thermal conductances in these four cases are shown in Figs. 3b & 3c. The results agree with good accuracy with the theoretical expectations¹.

The $\nu=5/2$ state may host different topological orders, with each having a different modes structure and a different thermal conductance⁵. Here, we consider the two competing candidates: PH-Pf and A-Pf (for a discussion of other possible orders, see Methods). Both orders support counterpropagating modes at the bare edge of the sample, i.e., the ‘5/2-0’ configuration (Figs. 4a-4b). Aside from two downstream integer modes, the PH-Pf order supports a downstream $\nu=1/2$ charge mode and an upstream Majorana mode. In comparison, the A-Pf order supports a downstream $\nu=1/2$ charge mode and three upstream Majorana modes (two Majorana modes form a single bosonic neutral mode). With counterpropagating modes, an accurate determination of the thermal equilibration between all modes is imperative. With complete (or no) thermal equilibration, one expects $2.5\kappa_0T$ ($3.5\kappa_0T$) for the PH-Pf and $1.5\kappa_0T$ ($4.5\kappa_0T$) for A-Pf.

Figures 4a-4f present different configurations: ‘5/2-0’, ‘5/2-1’, ‘5/2-2’. As shown in the figures, the expected two-terminal thermal conductance of the PH-Pf and A-Pf can overlap, considering the range from full equilibration to no equilibration. However, the interface ‘5/2-3’ points a clear distinction between the two topological orders (Fig. 4g-4h). Here, the A-Pf supports two copropagating modes; both leave the hot contact equilibrated at temperature T_m , with expected thermal conductance $1.5\kappa_0T$. By contrast, the PH-Pf order supports a counterpropagating $\nu=1/2$ charge mode and a Majorana mode, leading to thermal conductance in the range $0.5\kappa_0T - 1.5\kappa_0T$.

In Figs. 4i-4l, we present the measurement results of ΔP vs T_m^2 at the four 5/2-interfaces: ‘5/2-0’, ‘5/2-1’, ‘5/2-2’ and ‘5/2-3’. The measured thermal conductances are $(2.55 \pm 0.07)\kappa_0T$, $(1.53 \pm 0.04)\kappa_0T$, $(0.55 \pm 0.02)\kappa_0T$, and $(0.53 \pm 0.02)\kappa_0T$, respectively. These results point at the fully equilibrated PH-Pf order (Figs. 4a-4h). Most importantly, observing $KT \sim 0.5\kappa_0T$ in the ‘5/2-3’ interface is the decisive result that rules out the A-Pf order (see above), identifying the topological order of the $\nu=5/2$ agreeing with the PH-Pf. Note that the disorder in our shallow-DX centers doping may play a role in stabilizing this topological order^{1,2}. Above all, the observed $1/2$ -quanta thermal conductance proves a fully equilibrated $1/2$ downstream charge mode and an upstream Majorana mode, and hence unambiguously identify the non-abelian nature of the $\nu=5/2$ state.

Our work exploits a novel ‘*interfacing*’ method², which allows measuring the thermal conductance at the junction between two adjacent QHE states. The advantage of our interfacing method lies in the elimination of the integer modes, thus relaxing the ambiguity the thermal equilibration among multiple edge modes. The measurements of the thermal conductance at the interface between $\nu=5/2$ and

$\nu=\text{integers}^{26,27}$, assured a clear distinction between the competing orders, with the PH-Pf as the identified topological order and showed the unambiguous existence of non-abelian edge modes in $\nu=5/2$ state. Needless to say that this configuration can be readily applied to the construction of interferometers allowing non-abelian braiding operations, a necessary step in topological quantum processing.

References

- 1 Banerjee, M. *et al.* Observation of half-integer thermal Hall conductance. *Nature* **559**, 205-210, doi:10.1038/s41586-018-0184-1 (2018).
- 2 Dutta, B. *et al.* Novel method distinguishing between competing topological orders. *arXiv preprint arXiv:2101.01419* (2021).
- 3 Wen, X. G. Non-Abelian statistics in the fractional quantum Hall states. *Physical Review Letters* **66**, 802-805, doi:10.1103/PhysRevLett.66.802 (1991).
- 4 Pendry, J. B. Quantum limits to the flow of Information and entropy. *Journal of Physics a-Mathematical and General* **16**, 2161-2171, doi:10.1088/0305-4470/16/10/012 (1983).
- 5 Ma, K. K. W. & Feldman, D. E. The sixteenfold way and the quantum Hall effect at half-integer filling factors. *Phys. Rev. B* **100**, 035302, doi:10.1103/PhysRevB.100.035302 (2019).
- 6 Kane, C. L. & Fisher, M. P. A. Quantized thermal transport in the fractional quantum Hall effect. *Physical Review B* **55**, 15832-15837, doi:10.1103/PhysRevB.55.15832 (1997).
- 7 Gromov, A., Cho, G. Y., You, Y., Abanov, A. G. & Fradkin, E. Framing Anomaly in the Effective Theory of the Fractional Quantum Hall Effect. *Physical Review Letters* **114**, 016805, doi:10.1103/PhysRevLett.114.016805 (2015).
- 8 Morf, R. H. Transition from quantum Hall to compressible states in the second Landau Level: new light on the $\nu=5/2$ enigma. *Physical Review Letters* **80**, 1505-1508, doi:10.1103/PhysRevLett.80.1505 (1998).
- 9 Storni, M., Morf, R. H. & Das Sarma, S. Fractional quantum Hall state at $\nu=5/2$ and the Moore-Read pfaffian. *Physical Review Letters* **104**, 076803, doi:10.1103/PhysRevLett.104.076803 (2010).
- 10 Moore, G. & Read, N. Nonabelions in the fractional quantum Hall effect. *Nuclear Physics B* **360**, 362-396, doi:10.1016/0550-3213(91)90407-O (1991).
- 11 Levin, M., Halperin, B. I. & Rosenow, B. Particle-Hole Symmetry and the Pfaffian State. *Physical Review Letters* **99**, 236806, doi:10.1103/PhysRevLett.99.236806 (2007).
- 12 Lee, S. S., Ryu, S., Nayak, C. & Fisher, M. P. Particle-hole symmetry and the $\nu = 5/2$ quantum Hall state. *Physical Review Letters* **99**, 236807, doi:10.1103/PhysRevLett.99.236807 (2007).
- 13 Bid, A. *et al.* Observation of neutral modes in the fractional quantum Hall regime. *Nature* **466**, 585-590, doi:10.1038/nature09277 (2010).
- 14 Gross, Y., Dolev, M., Heiblum, M., Umansky, V. & Mahalu, D. Upstream neutral modes in the fractional quantum Hall effect regime: Heat waves or coherent dipoles. *Physical Review Letters* **108**, 226801, doi:10.1103/PhysRevLett.108.226801 (2012).
- 15 Zaletel, M. P., Mong, R. S. K., Pollmann, F. & Rezayi, E. H. Infinite density matrix renormalization group for multicomponent quantum Hall systems. *Physical Review B* **91**, 12, doi:10.1103/PhysRevB.91.045115 (2015).
- 16 Rezayi, E. H. Landau Level mixing and the ground state of the $\nu=5/2$ quantum Hall effect. *Physical Review Letters* **119**, 026801, doi:10.1103/PhysRevLett.119.026801 (2017).
- 17 Zucker, P. T. & Feldman, D. E. Stabilization of the particle-hole pfaffian order by Landau-Level mixing and impurities that break particle-hole symmetry. *Physical Review Letters* **117**, 096802, doi:10.1103/PhysRevLett.117.096802 (2016).
- 18 Mross, D. F., Oreg, Y., Stern, A., Margalit, G. & Heiblum, M. Theory of disorder-induced half-integer thermal Hall conductance. *Physical Review Letters* **121**, 026801, doi:10.1103/PhysRevLett.121.026801 (2018).
- 19 Wang, C., Vishwanath, A. & Halperin, B. I. Topological order from disorder and the quantized Hall thermal metal: Possible applications to the $\nu=5/2$ state. *Physical Review B* **98**, 045112, doi:10.1103/PhysRevB.98.045112 (2018).

- 20 Fulga, I. C., Oreg, Y., Mirlin, A. D., Stern, A. & Mross, D. F. Temperature Enhancement of Thermal Hall Conductance Quantization. *Physical Review Letters* **125**, 236802, doi:10.1103/PhysRevLett.125.236802 (2020).
- 21 Lian, B. & Wang, J. Theory of the disordered $\nu=5/2$ quantum thermal Hall state: Emergent symmetry and phase diagram. *Physical Review B* **97**, doi:10.1103/PhysRevB.97.165124 (2018).
- 22 Simon, S. H. Interpretation of thermal conductance of the $\nu = 5/2$ edge. *Physical Review B* **97**, 121406, doi:10.1103/PhysRevB.97.121406 (2018).
- 23 Feldman, D. E. Comment on "Interpretation of thermal conductance of the $\nu=5/2$ edge". *Physical Review B* **98**, 167401, doi:10.1103/PhysRevB.98.167401 (2018).
- 24 Simon, S. H. & Rosenow, B. Partial Equilibration of the Anti-Pfaffian Edge due to Majorana Disorder. *Physical Review Letters* **124**, 126801, doi:10.1103/PhysRevLett.124.126801 (2020).
- 25 Ma, K. K. W. & Feldman, D. E. Thermal Equilibration on the Edges of Topological Liquids. *Physical Review Letters* **125**, doi:10.1103/PhysRevLett.125.016801 (2020).
- 26 Jezouin, S. *et al.* Quantum limit of heat flow across a single electronic channel. *Science* **342**, 601-604, doi:10.1126/science.1241912 (2013).
- 27 Banerjee, M. *et al.* Observed quantization of anyonic heat flow. *Nature* **545**, 75-79, doi:10.1038/nature22052 (2017).
- 28 Umansky, V. & Heiblum, M. *MBE growth of high-mobility 2DEG*. (Elsevier Science BV, 2013).
- 29 Goerbig, M. O., Lederer, P. & Morais Smith, C. Microscopic theory of the reentrant integer quantum Hall effect in the first and second excited Landau levels. *Physical Review B* **68**, 241302, doi:10.1103/PhysRevB.68.241302 (2003).

Acknowledgments

We acknowledge D. Mross and M. Banerjee for a critical reading of the manuscript, followed by useful suggestions. B.D. acknowledges the support from Clore Foundation. M.H. acknowledges the continuous support of the Sub-Micron Center staff, the support of the European Research Council under the European Community's Seventh Framework Program (FP7/2007-2013)/ERC under grant agreement number 713351, the partial support of the Minerva foundation under grant number 713534.

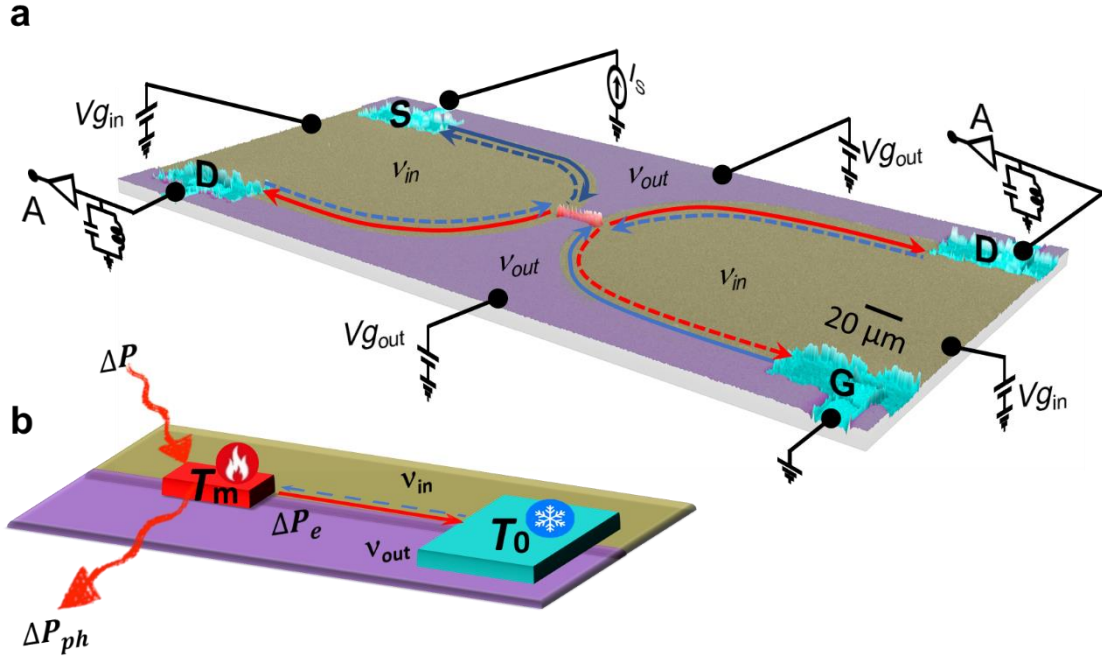


Figure 1 | The experimental setup used to measure the interface thermal conductance. a, False colored SEM micrograph of the heart of the device. Two biased top gates, inner-gate ($V_{g_{in}}$, yellow) and outer-gate ($V_{g_{out}}$, violet), divide the 2DEG mesa into two gate-defined arms. A small floating ohmic contact (red, dimensions $20 \times 2 \mu\text{m}^2$) connects the two arms. Large contacts (S, D, G, in cyan) probe the interface filling. Added ohmic contacts at the edge of MESA (not shown here) probe the filling of the respective sides. The floating contact is heated to T_m by an injecting current I_s from S. Its temperature is determined by measuring the low-frequency Johnson-Nyquist noise at 630kHz (LC bandwidth 10-30kHz), after amplification by a cooled pre-amplifier (at 4.2K) followed by a room-temperature amplifier. Arrows indicate the interface-modes at '5/2-3' interface as an example (see Fig. 4). **b,** Schematic representation of heat balance in the floating contact, with the same color-codes as in **a**, showing only a zoomed-in part of the interface along downstream. An injected current dissipates power ΔP , which is evacuated by two main channels: the phononic channel ΔP_{ph} and the electronic channel ΔP_e . The cold reservoir contact G is at temperature T_0 . Due to the small volume of the floating contact, the phononic contribution is negligible at low temperatures.

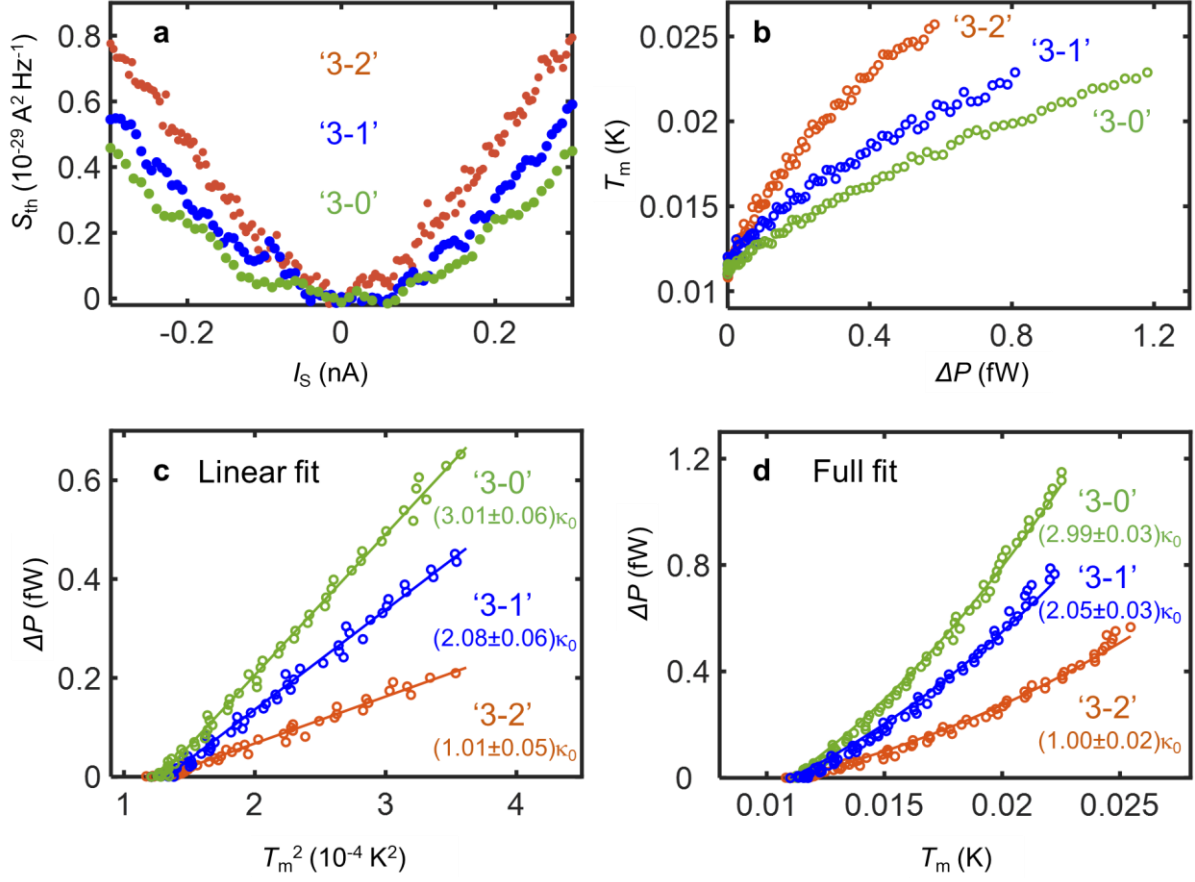


Figure 2 | Noise, temperature, and dissipation at integer interfaces. **a**, Excess Johnson-Nyquist noise S_{th} as function with heating current I_s for the three 'integer interfaces': '3-2' (orange), '3-1' (blue), and '3-0' (green) at $T_0=11\text{mK}$. **b**, Calculated temperature T_m as a function of the dissipated power $\Delta P = 0.25I_s^2 R_s$, with R_s the 'interface mode' resistance, for the three different configurations (see Methods). **c**, Dissipated power as a function of squared temperature in the range $T_m < 18\text{mK}$. The thermal conductance is determined from the slope, via $\Delta P = \frac{1}{2}K(T_m^2 - T_0^2)$. **d**, Dissipated power as a function of temperature in the range $T_m < 30\text{mK}$. Here, phonon contribution is included, via $\Delta P = \frac{1}{2}\kappa(T_m^2 - T_0^2) + \beta(T_m^5 - T_0^5)$, with e-ph coupling constant $\beta \approx 5 \times 10^9 \text{ WK}^{-5}$.

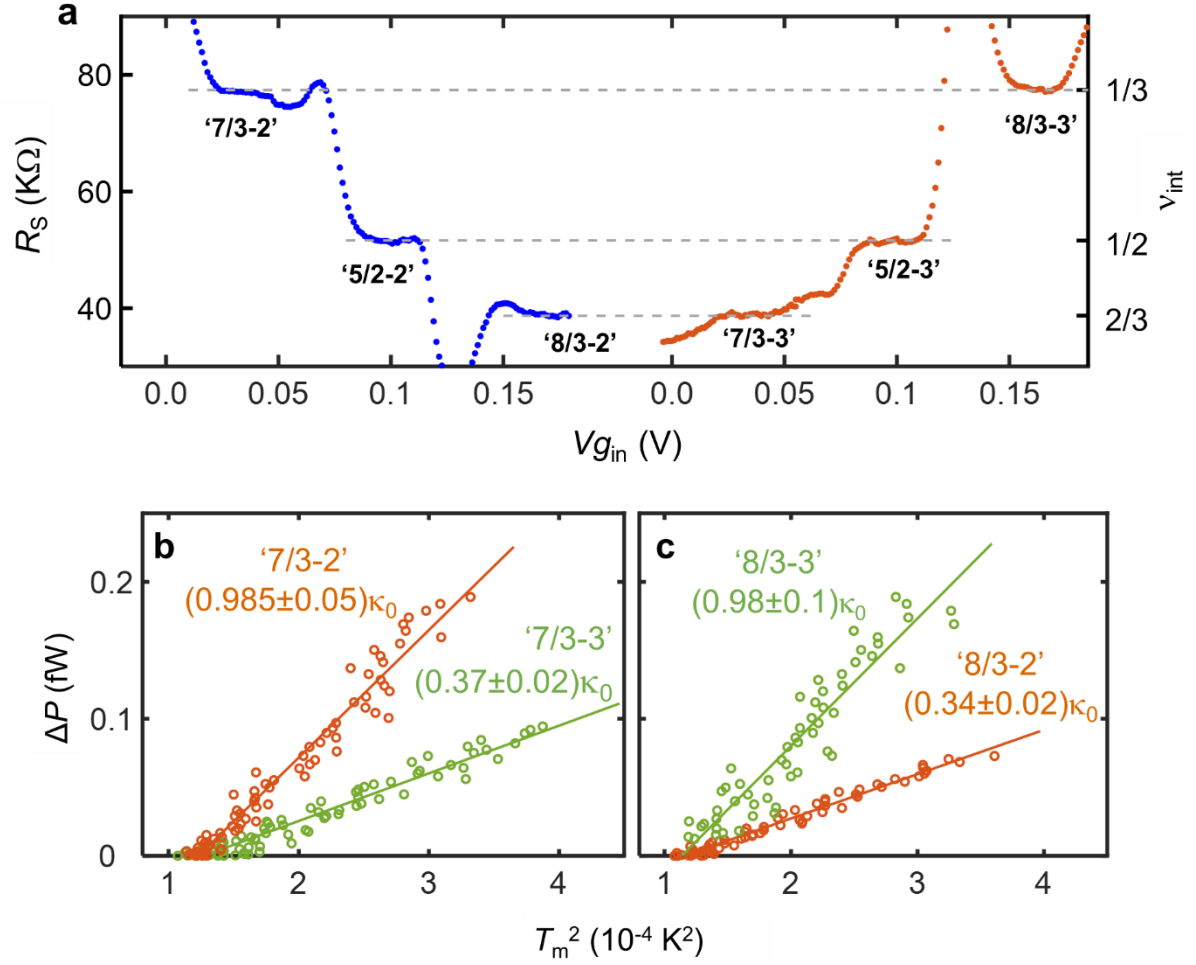


Figure 3 | Interface resistance and thermal conductance of states in the 2nd LL. **a**, Two terminal source interface resistance of '7/3-2&3', '5/2-2&3', and '8/3-2&3'. Quantized plateaus indicate full charge equilibration at the interface. The peaks and dips are attributed to reentrant effects²⁹. **b**, Determination of the thermal conductance for $T_m < 18$ mK, as was done in **Figure 2**. The slope for '7/3-2' is close to unity, as expected for the 1/3 interface mode. The slope for '7/3-3' is $0.37\kappa_0$, and not zero - due to the well-known lack of equilibration of the resultant 2/3 mode²⁷. **c**, Similar data to **b** at different interfacing conditions with $\nu=8/3$.

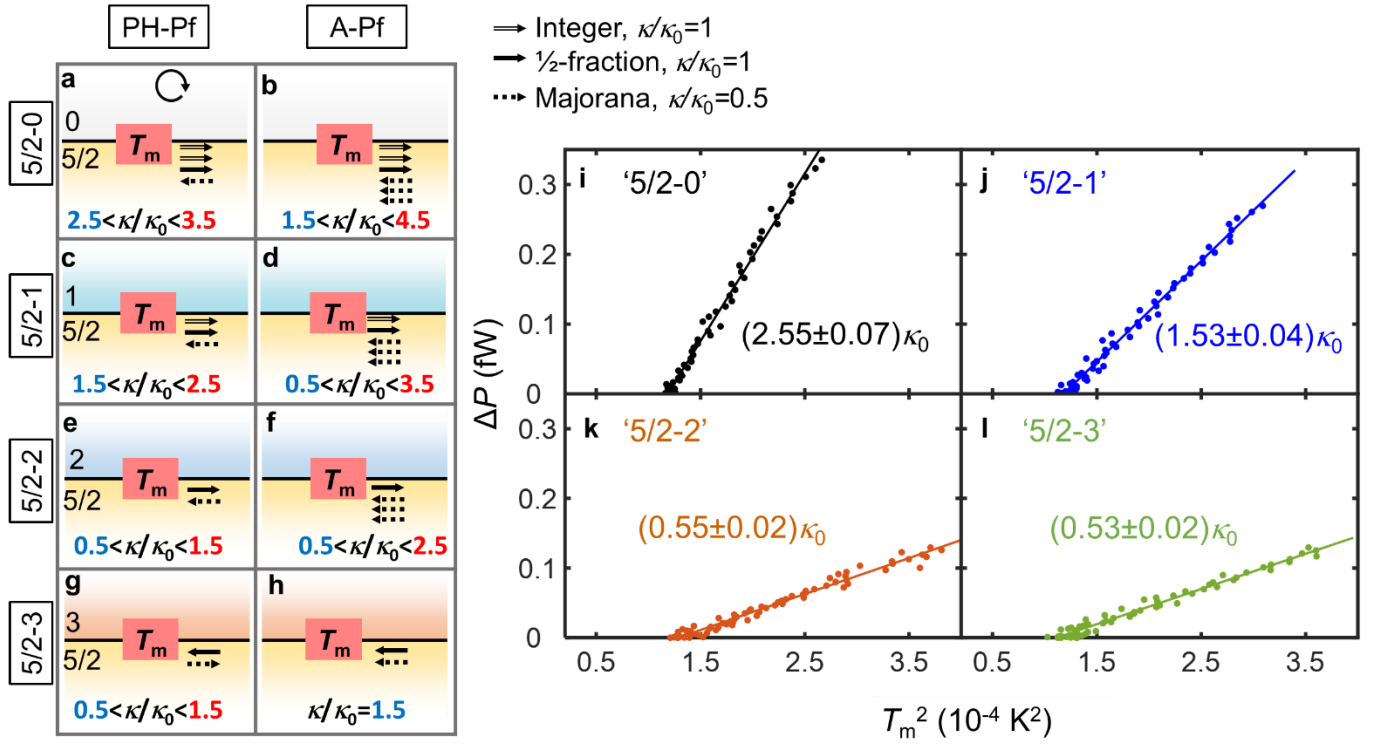


Figure 4 | Thermal conductance of the '5/2-n' interfaces. a-h, Plotted are the interface modes of the interfaced PH-Pf and the A-Pf orders with different integers, and the expected thermal conductance in each case. Fully-equilibrated value in light-blue and un-equilibrated value in red. Notation of the arrows are indicated in the inset. Clockwise chirality is indicated by the circled arrow. i-l, Linear plots as in Figs. 2 & 3. The extracted thermal conductance values, in particular for '5/2-3', unambiguously exclude the A-Pf topological order, and agrees (with small estimated errors) with the Ph-Pf topological order.

METHODS

MBE-grown ‘inverted’ heterostructure. The heterostructures used in these experiments were designed to achieve a compromise between the robustness of the 5/2 fractional state and the ability to operate it with surface gates. It is well established that a quantization of the 5/2 state is governed by the long-range spatial potential landscape formed by the ionized donors. Smoothing this landscape is customarily achieved by excessive doping, either in ‘short period superlattice’²⁸, or in a low Al-mole-fraction in AlGaAs¹. These doping schemes provide a significant reduction in the long-range potential fluctuations via spatial correlations between ionized donors, exhibiting, at the same time, negligible lateral parasitic conductance at low temperatures. Unfortunately, weakly localized electrons in such doped layers both thwart the stable operation of the surface gates and completely inhibit applying positive gate bias, which is essential in the present experiment. In order to solve the problem, we use the so-called ‘inverted’ 2DEG structure, where an accurate quantization of the 5/2 state is enabled by excess δ -doping in a layer of $\text{Al}_x\text{Ga}_{1-x}\text{As}$ ($x=0.23$) placed 65nm (or 70nm) *below* the QW (see [Extended Data Fig. 1](#)). The surface potential is compensated using a uniformly doped layer made of $\text{Al}_{0.37}\text{Ga}_{0.63}\text{As}:\text{Si}$, located far away from the QW, thus minimizing the impact of its long-range random potential fluctuations on the 2DEG. Such high Al mole-fraction doped layers are conventionally used between the gates and the 2DEG in most devices since the electrons freeze at $T \sim 100\text{K}$ in the DX-Si centers. The electron density in as-grown samples at 300mK is $\sim 2.4 \times 10^{11} \text{cm}^{-2}$ and the mobility is $15 \times 10^6 \text{cm}^2/\text{Vs}$, even though the 2DEG wavefunction is asymmetrically shifted towards the bottom AlGaAs-GaAs interface - usually considered to be of lower quality than the top interface of the quantum well.

Device fabrication. We start with a $250 \times 800 \mu\text{m}$ MESA, made by wet etching in $\text{H}_2\text{O}_2:\text{H}_3\text{PO}_4:\text{H}_2\text{O}=1:1:50$ solution for 2 mins resulting with etched depth of about 180 nm. In the next step, a few ohmic contacts are patterned by e-beam-lithography at the edge and in the bulk of the MESA, followed forming the ohmic contacts by metal deposition (with standard material ratio $\text{Au}:\text{Ge}:\text{Ni} = 2:1:0.75$), followed by annealing at 450°C for 2 mins. Some of the contacts are shown in [Fig. 1a](#) as S, G, D contacts. The whole sample is then coated with 25 nm of HfO_2 layer via ALD, acting as dielectric medium for the metallic-gate that follows. In the next step, the outer-gate ($V_{g_{\text{out}}}$) is patterned by e-beam-lithography and subsequently deposited a 20 nm Ti/Au thin metallic film, acting as the outer-gate. We then coat the sample with another 15 nm thick of HfO_2 layer, which separates the outer-gate from the following inner-gate. Next step consist of patterning of inner-gate ($V_{g_{\text{in}}}$) and subsequent metallization by 20 nm Ti/Au thin film. The ohmic contacts (such as S, G, D) in the bulk of the MESA were designed such that they sit exactly at the interface of the two gates. In

the final step, the interface-ohmic contacts (like, S, D, G contacts) are connected to the bonding-pads by thick gold lines, passing over the HfO₂ covered outer-gate, such that they do not short to the gates.

Experimental setup. The heart of the device is shown in Fig. 1a. Gate voltages ($V_{g_{in}}$ and $V_{g_{out}}$) are applied to divide the mesa into two gate-defined arms. The small-floating ohmic contact with area $20 \times 2 \mu\text{m}^2$ act as the floating hot-reservoir connecting the two arms. An injected DC current I_s from the interface-contact 'S' heats up the floating contact to temperature T_m . The voltage amplifiers are connected to the drain contact 'D' at the interface. Thermal voltage fluctuations (S_v) of the hot-floating contact is measured by the amplifiers after being filtered by the LC resonant circuit. The voltage fluctuations are converted into current fluctuations as $S_{th} = S_v G_{int}^2$, with G_{int} the conductance of the interface mode.

In the following we give an example, which describes the experimental process for the measurements at the 5/2-interfaces. First, the magnetic field is tuned to a value $B \approx (-/+)$ 4T (chirality clockwise/anti-clockwise). At this magnetic field, with the bare density ($n \sim 2.4 \times 10^{11} \text{cm}^{-2}$) the whole sample remains at a filling $\nu > 2$, just outside the $\nu=2$ plateau. Now, we create 5/2-interfaces by tuning the gates. For making '5/2-n' interface, where, $n=2,1,0$ (at $B=-4\text{T}$), we apply positive gate voltage $V_{g_{in}}$ to populate the inner-gated region to $\nu_{in}=5/2$, while apply a negative gate voltage $V_{g_{out}}$ on the outer-gate to deplete the outer-gated region to $\nu_{out}=2, 1$, or fully pinch to $\nu_{out}=0$. Similarly, for making '5/2-3' interface (at $B=+4\text{T}$; with a fixed amplifier position we needed to reverse B to $+4\text{T}$, to have the amplifier on the downstream side), we apply certain positive gate voltages on both gates to populate the inner-gated regions to $\nu_{in}=5/2$, and the outer-gated region to $\nu_{out}=3$, respectively. Secondly, to characterize the 'interface-mode', we measure the 2-terminal resistance at the interface ohmic contacts (e.g., at 'S'). Nicely quantized interface-resistance ensures proper charge equilibration. Next, we measure the branching of the impinging current at the floating Ohmic contact. We assure symmetric partitions of the current between the two arms, with less than 2% reflections. After this, we proceed for the thermal conductance measurements at the interface.

Determination of amplifier Gain and T_0 . The gain of the amplifier is a crucial parameter to determine the temperature T_m of the floating-contact. We take the advantage of the temperature dependent Johnson-Nyquist voltage noise of the well-known Hall-resistance R_s of the interface modes to calibrate the gain of amplifier. The equilibrium voltage noise of the R_s (well-known with good accuracy) is measured at the central frequency ($f_0 \sim 630\text{KHz}$) of the LC resonant circuit, with a Δf bandwidth opened at the spectrum analyzer, for different cryostat (bath) temperatures T_{bath} measured by well calibrated commercial thermometers, $S_v = 4k_B R_s T_{bath} G_h^2 G_c^2 \Delta f + S_{const}$, where k_B , the Boltzmann constant; $G_h=400$, the known gain of the room-temperature amplifier; and S_{const} is the temperature independent voltage noise of the

amplifier. A plot of the normalized voltage noise, $S_{\text{norm}} = S_V / (4k_B R_S G_h \Delta f)$, at the '2-1' interface, with different bath temperatures is shown in **Extended Data Fig. 2**. The slope of the linear fit of the data gives the gain of the cold amplifier, $G_c = \sqrt{\Delta S_{\text{norm}} / \Delta T}$. The obtained gain at this interface is $G_c \sim 7.7$, which is actually the effective gain of the amplifier depending on the particular bandwidth of the LC circuit. For different interface modes the bandwidth (depends on R_S) of the circuit changes and so the effective gain of the amplifier. The ratio of the areas of resonance curves for two interfaces is directly proportional to the ratio of the squared gains in the two cases. The area under the LC resonance curves for two interfaces (with two different R_S) were compared to extract the gain at different interface fillings.

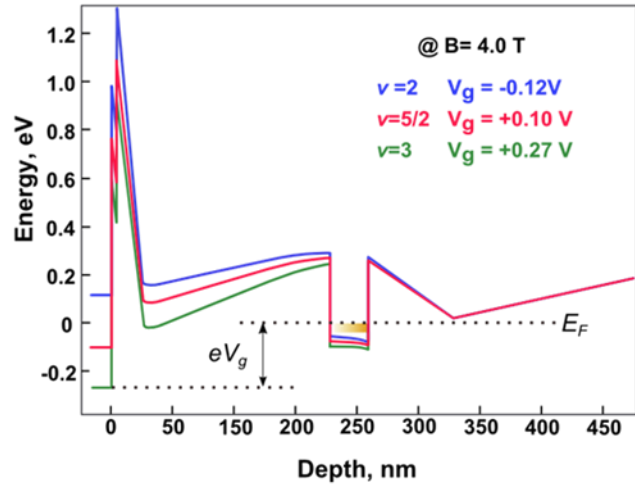
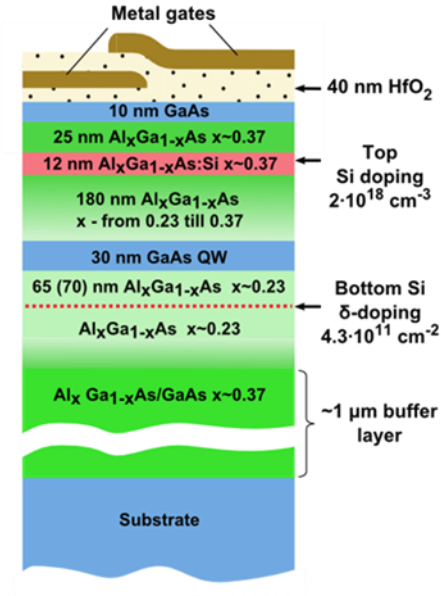
After knowing the gain of the amplifier, the temperature T_0 is inferred from the above calibration curve, by measuring the thermal-background noise of the interface resistances.

Determination of T_m . We extract the temperature T_m of the small-floating contact by measuring the excess thermal fluctuations from the floating contact carried out by the interface edge modes. Using the general expression for the excess current noise S_{th} , carried out by n_1 and n_2 number edge channels in the two arms, we get the temperature of the floating contact T_m given by,

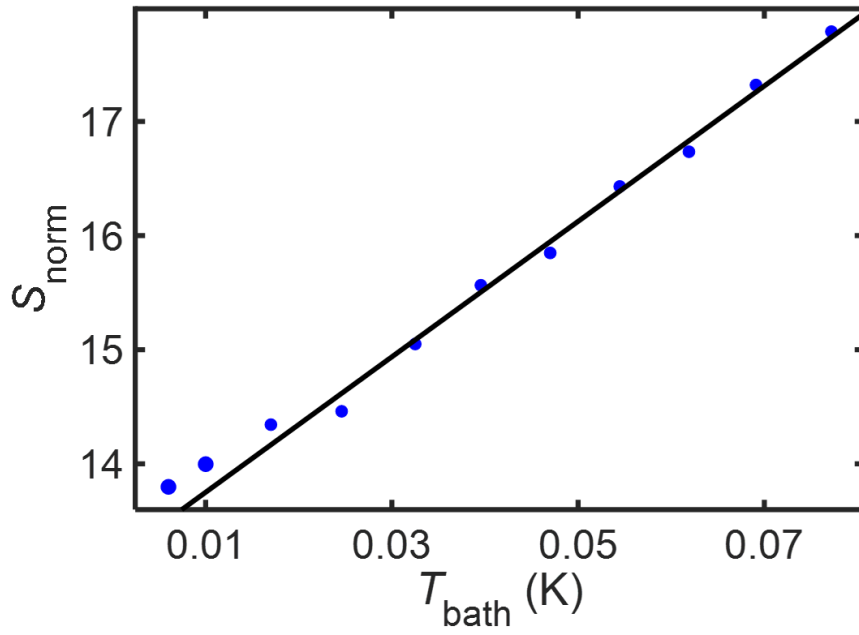
$$T_m = T_0 + S_{\text{th}} / 2k_B G^*,$$

Where, $G^* = G_{\text{int}} \frac{n_2(n-n_2)}{n}$, with $n = n_1 + n_2$, and G_{int} is the conductance of the interface mode. In our case $n_1 = n_2$, therefore, $G^* = \frac{1}{2} G_{\text{int}}$.

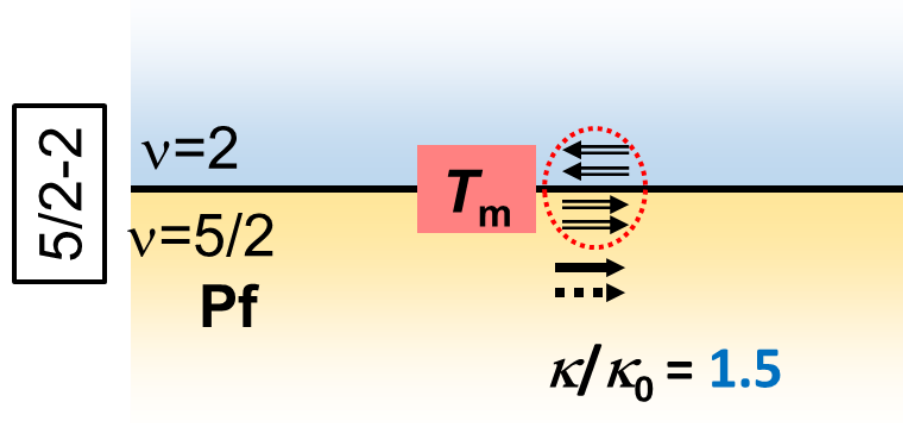
5/2-interface thermal conductance for other possible topological orders. In the main text we have considered PH-Pf and A-Pf topological orders of $\nu=5/2$ state. The Pf order (**Extended Data Fig. 3**), which supports a DS Majorana mode, is also numerically favorable. But the observation of US noise makes it experimentally unlikely. Still, at the interface of the Pf-order with $\nu=2$ (**Extended Data Fig. 3**) one expects a definite value of thermal conductance $KT=1.5\kappa_0 T$, which doesn't match the observed value in our experiment, $KT \cong 0.5\kappa_0 T$ (see **Fig. 4k**). Therefore, we can exclude the Pf order. Similarly all other a-priori possible topological orders can be excluded either by the interface with $\nu=2$ or with $\nu=3$ ⁵.



Extended Data Figure 1 | MBE growth structure of the heterostructure. **left**, Cross-section of the MBE growth (not in scale). **right**, Conduction band at three different gate voltages corresponding to three different filling factors $\nu=2$, $5/2$, and 3 .



Extended Data Figure 2 | Calibration of the amplifier. Temperature-dependent Johnson-Nyquist noise of the interface resistance R_s allows calibration of the amplifier. The normalized noise at the '2-1' interface is plotted with the bath temperature. The slope of the linear fit gives the gain of the amplifier for this interface.



Extended Data Figure 3 | expected interface thermal conductance for ‘5/2-2’ interface with the Pf topological order. At the interface of $\nu=5/2$ -Pf order with $\nu=2$, two integer modes are gapped out, leaving at the interface $\nu=1/2$ and a Majorana mode both in the DS, hence, thermally equilibrated at T_m . The expected thermal conductance is $1.5\kappa_0T$, in disagreement with the experimentally observed value(Fig. 4k).